

The effects of DiloCarB as carbonation accelerator on the properties of lime mortars

Duygu Ergenç  · Rafael Fort  · António Santos Silva  · Rosário Veiga  · David Sanz Arauz

Received: 13 August 2017 / Accepted: 8 January 2018 / Published online: 12 January 2018
© RILEM 2018

Abstract This study investigates the effect of the diethyl carbonate as a carbonation accelerator on the carbonation of lime mortars. Two types of lime mortars were prepared, one using lime putty and standard sand and the other using lime putty, dust and fragments of ceramic and standard sand. After a curing time of two weeks, the accelerator product, diethyl carbonate in a solution of ethanol and water, was sprayed on half of the mortars of each type. The differences in the carbonation performance were analyzed at 28, 90, 120 and 180 days using different analytical methods. Apart from the mineralogical and petrographic characterization, the physical, mechanical and hydric properties of the samples were determined. Mechanical tests were conducted only at 90,

120 and 180 days, because at 28 days the lime mortars were considered still too soft. The mortar samples with the accelerator had steadier carbonation and slight changes in their microstructure.

Keywords Carbonation accelerator · Ceramic aggregate · XRD · TGA–DSC · SEM/EDS · MIP · Physical–mechanical properties

1 Introduction

The restoration of historical buildings using lime mortars is getting more common everyday due to their compatibility with the preexisting materials. The complete transformation of calcium hydroxide (portlandite, $\text{Ca}(\text{OH})_2$) to calcium carbonate (calcite, CaCO_3) can be a very slow process, depending on the environmental conditions. Therefore, the lime could need months or years to totally react with atmospheric carbon dioxide [1], and many factors, including maturation of lime putty, pore size distribution, relative humidity and temperature and thickness of the mortar element, affect the effectiveness of the carbonation process [2–4]. There have been some precedent cases of historic mortars kept non-carbonated inside masonry [5, 6]. The setting time of lime mortars is too long for modern construction, which favors the use of Portland cement–lime and gypsum–lime mixes because they set quickly [7–11]. However,

D. Ergenç (✉) · R. Fort
Institute of Geosciences (CSIC-UCM), Calle Severo
Ochoa, 7, 28040 Madrid, Spain
e-mail: duyguergenc@ucm.es

D. Ergenç
Conservation and Restoration of Architectural Heritage
Program, E.T.S.A.M, UPM, Av. Juan de Herrera, 4,
28040 Madrid, Spain

A. Santos Silva · R. Veiga
National Laboratory for Civil Engineering, Av. do Brasil
101, 1700-066 Lisbon, Portugal

D. Sanz Arauz
Construction and Architectural Technology Department,
E.T.S.A.M, UPM, Av. Juan de Herrera, 4, 28040 Madrid,
Spain

the incorporation of these binders in old masonries creates problems even in small proportions, as they generate harmful soluble salts, such as sulphates and chlorides, leading to formations of expansive compounds in the presence of water. In addition, the higher mechanical strength and stiffness as well as higher dilatation coefficient of cement-based mortars prevent the masonry from moving in harmony. Also, smaller pores of cement mortars produce water retention in the interfaces with the more permeable preexistent materials [10, 12–17]. Therefore, it is necessary to search for other additives that promote the carbonation process of calcium hydroxide and improve the physical and mechanical properties of lime mortars.

It is known that in antiquity some additives were added in the manufacturing of lime mortars in order to improve their properties [18–20]. Today, different types of additives are used and tested, including artificial pozzolans (e.g., ceramic waste, fly ash, silica fume, metakaolin and calcined clays) [21–27], chemical admixtures such as air entraining, water-retaining (cellulose derivative) and water repellent agents [28, 29], plasticizers (e.g., polycarboxylate) [30, 31], organic additives [32, 33] and nanoparticles of calcium hydroxide, silica, titania and alumina [34–36].

Various combinations of lime powder, lime putty, additives, aggregates, water/binder ratio and curing conditions had been used by different researchers, in which periodic measurements were carried out using phenolphthalein, capillary absorption, saturation, pore size distribution, mechanical tests and thermogravimetric analyses to evaluate the carbonation reaction kinetics [27, 29, 31–47].

The acceleration of the setting process to increase the carbonation rate is an important way to improve mortar performance. Different processes and/or additives causing rapid carbonation have been studied by scholars. The use of ethylenediaminetetraacetic acid (EDTA, $C_{10}H_{16}N_2O_8$) [48] or terpineol ($C_{10}H_{18}O$) [49] are known to improve carbonation velocity rate due to high CO_2 absorption.

Diethyl carbonate (DEC, $C_5H_{10}O_3$), also known as carbonate ester of carbonic acid, can accelerate carbonation as well. The diethyl carbonate solution in ethanol (C_2H_5OH) and water (H_2O) carbonates under alkaline conditions. When it encounters calcium hydroxide ($Ca(OH)_2$), the DEC decomposes to ethanol and carbonate ions that react with calcium ions to form calcium carbonate. This reaction enables faster

carbonation by atmospheric CO_2 and carbonation even with limited air exposure [37].

The aim of this research is to assess the effectiveness of the use of a diethyl carbonate additive for accelerating the carbonation of lime mortars prepared with standard siliceous sand and with ceramic as a partial replacement of the siliceous sand.

2 Materials and methods

2.1 Preparation of the samples

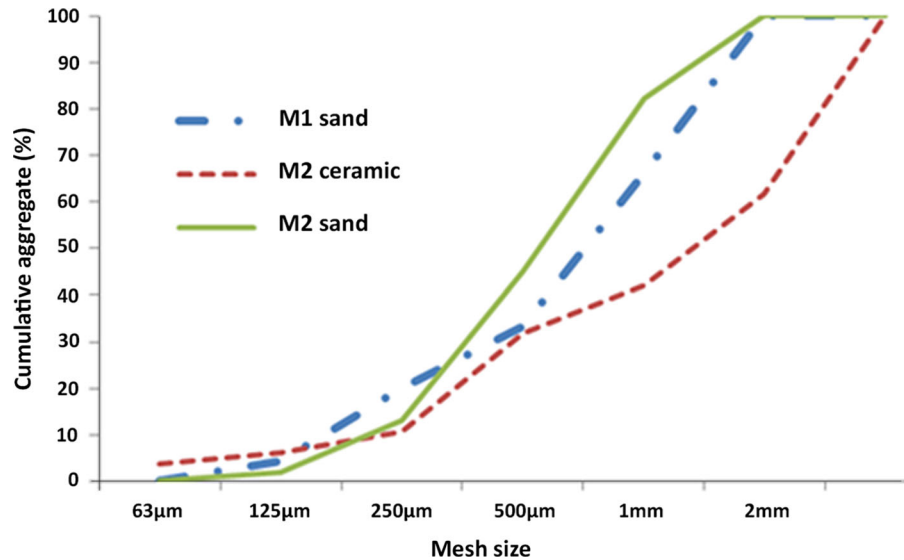
Two kinds of mortar mixture were prepared: one with calcitic lime putty and siliceous sand (M1) and another using the same materials, but with ceramic aggregate as a partial replacement for the sand (M2). The formulation of these mortars was done taking into account the data obtained from the characterization of the Roman mortars of the Complutum archaeological site (Alcalá de Henares, Spain) [50]. The proportion of the M1 mortar mix was 1:3 (lime putty: sand), and that of the M2 mortars was 1:0.5:1:2 (lime putty: ceramic dust: ceramic fragments: sand). The water content of the lime putty was 85%, and the water/binder ratios were 0.5 in both mixes. The apparent densities of the ceramic, sand and lime putties were 1.33, 1.48 and 1.36 g/cm^3 , respectively.

To prepare the mortar mixtures, lime putty produced by PROEISCON Ltd., standard siliceous sand (EN 196-1) and Roman ceramics from Complutum, that were crushed and sieved according to the grain size of the *opus signinum* mortars in the site [50], were used (Fig. 1).

For the mechanical mixing, the aggregates were first introduced into the vessel, then the lime putty, both were mixed, and finally water was added slowly as much as needed until adequate workability was obtained, verified by experimental application; the M1 mix had $120 \pm 2.3\text{ mm}$, and the M2 mix had $130 \pm 1.8\text{ mm}$ diameter on the flow table. Specimens of the two mortar types were prepared, namely prismatic specimens of $160 \times 40 \times 40\text{ mm}^3$, molded according to EN 1015-12 [51], which were manually filled into the metallic molds with high attention to smoothness and compactness. All these specimens were left in an open chamber in the laboratory with monitored temperature (T) relative humidity (RH) and



Fig. 1 Grain size distribution of the sand and ceramic aggregates



carbon dioxide (CO_2), average 25 ± 3 °C, $34 \pm 8\%$ and 703 ± 116 ppm, respectively.

Two weeks later, the specimens were removed from the molds, and a total of 64 specimens by each mortar type were used. The diethyl carbonate (DEC) accelerator product DiloCarB[®], was sprayed on half of the M1 and M2 mortar specimens, which were then covered with damp cloths for 5 h to allow full exposure to the solution.

The nomenclature for the samples designates the mixture type (M1, M2), the curing conditions (L: laboratory, LA: laboratory with accelerator) and the age of carbonation at 28, 90, 120 and 180 days.

2.2 Experimental methodology

The specimens of treated and untreated mortar mixes were characterized by different analytical techniques, including X-ray diffraction (XRD), simultaneous thermal analysis (TGA–DSC), scanning electron microscopy coupled with energy dispersive X-ray spectroscopy (SEM/EDS) and mercury intrusion porosimetry (MIP). Water absorption capillarity, water saturation, surface hardness and air permeability were also measured. Then, ultrasonic velocities were measured before mechanical tests, and finally, the halves of the samples that were broken in the flexural strength test were used to determine compressive strength. With exception of the mechanical tests, which were not carried out at 28 days due to the poor

carbonation state and low mechanical resistance [10, 43], the remaining tests were done at the curing ages of 28, 90, 120 and 180 days.

In every group and curing age, one centimeter wide slices were cut from four centimeters inside the mortar prisms. These slices were cut into four equal pieces for use in the XRD, TGA–DSC, SEM–EDS and MIP analyses.

XRD analysis was done in a Bruker D8 Advance X-ray diffractometer fitted with a copper anode tube, a graphite monochromator and PC-ADP diffraction software. XRD patterns were acquired operating at 40 kV and 30 mA at 2θ angles of 2 – 68° with a 0.020 -step scan at a speed of 2° per minute. XRD diffractograms were done on powder particles (< 50 µm), and the data were analyzed using PANalytical X'Pert High Score X-ray diffraction analysis software and Joint Committee on Power Diffraction File database (JCPDF).

TGA–DSC was performed with a TA Instruments SDT-Q600 thermal analyzer in a nitrogen atmosphere at a heating rate of 10 °C/min. The data were processed using TA Instruments Universal Analysis DuPont 2000.

SEM/EDS studies were performed on a JEOL JSM 6400 scanning electron microscope fitted with an Oxford-Link Pentafet energy dispersive X-ray micro-analyzer on gold-coated broken samples.

Bulk and apparent density, open and total porosity were determined by water vacuum saturation according to UNE-EN 1936: 2007 [52, 53].

Pore size distributions were determined using MIP technique with the Micromeritics' AutoPore IV 9500 Series.

Water absorption tests were performed using the capillary absorption experiment according to UNE-EN 1015-18 [54].

Flexural and compressive strength tests were performed according to UNE-EN 1015-11:2007 [55].

Surface hardness values were measured using Equotip Proceq, which has an energy impact of 11 Nm. The 10 downward measurements were taken vertical and perpendicular to the sample surface [56, 57]. The hardness value is expressed as the Leeb number (L) or Leeb hardness (LH), which is the ratio of the rebound velocity to the impact velocity multiplied by 1000.

Air permeability of the mortars was measured by Permeameter Tiny-Perm-II Vindum Engineering [58].

Ultrasonic pulse velocity (UPV) was determined according the standard UNE 83-308-86 [59], and 5 direct measurements on 3 axes of the samples were taken with a PUNDIT CNS ELECTRONICS portable analyzer fitted with 1 MHz, 9 mm diameter transducers and utilizing coupling plasticine.

For the mechanical, physical and hydric experiments, three specimens from each group were utilized. In the UPV experiments, the specimens were measured before breaking in the mechanical tests. In other words, for each mortar group 9 specimens were tested at 28 and 90 days, 6 specimens at 120 days and 3 specimens at 180 days. The values presented are the average values of the tested samples.

3 Results and discussion

3.1 Mineralogical and thermal properties

Figure 2 shows the XRD results of the two mortar mixes with and without DEC (M1LA and M2LA, M1L and M2L, respectively). The main mineralogical constituents in the mortars are quartz and feldspar, from the siliceous sand that was used as aggregate, together with portlandite and calcite from the binder. Mica (biotite and muscovite), hematite and gehlenite,

together with a well-marked hump due to the amorphous mineral phases were detected in the specimens with ceramics (M2), which reflects the clay minerals from the Roman tiles and bricks that were used.

Calcite is expected to increase with curing age; however, the carbonation was low according to the diffractograms, since portlandite was present at 180 days, and the change in calcite was not remarkable. While there was a very slight increase in calcite peaks in every sample, and the highest intensity of calcite peak was reached at 180 days in the LA mortars. The decrease in portlandite peaks at 120 days was observed better in the LA samples (Fig. 2). The unreacted portlandite peaks indicate that the carbonation reactions did not consume all of the $\text{Ca}(\text{OH})_2$.

Vaterite,¹ a metastable polymorph of CaCO_3 with hexagonal symmetry, was detected in the X-ray diffraction patterns. In addition, the presence of aragonite,² the orthorhombic variety of CaCO_3 , more stable than the vaterite phase, was also detected both in the sample treated with DEC (LA sample) and in the sample without any treatment (the L sample), but subjected to laboratory conditions. In the M1L sample at 28 days, vaterite, then aragonite at 90 days, were seen, and at later stages, no peaks of metastable polymorphs were seen. The absence of peaks does not mean the absence of these minerals. It shows that their concentration was not high enough to pass the XRD detection limit (usually 2–5%). The same situation was observed in M1LA. The only difference was two aragonite peaks at 120 days. In the samples with ceramic inclusion, the L and LA samples had high amounts of aragonite at all stages. Considering the fact that vaterite is less stable than aragonite, the mortars with ceramic inclusion had improved carbonation with abundant aragonite peaks. Among the M2 mortars, a slightly more stable carbonation can be inferred from LA samples due to the presence of aragonite and calcite.

With the results of TGA–DSC analysis, the free portlandite and newly forming calcite contents were calculated based on the studies by researchers [43, 44, 60–66]. According to this approach, weight losses below 200 °C can be associated to the presence of hygroscopic water or hydrated compounds, while

¹ (JCPDF = 33-0268, $a = 7.147$, $c = 16.61\text{\AA}$).

² (JCPDF = 760606, $A = 4.959$, $b = 7.964$, 5.737\AA).



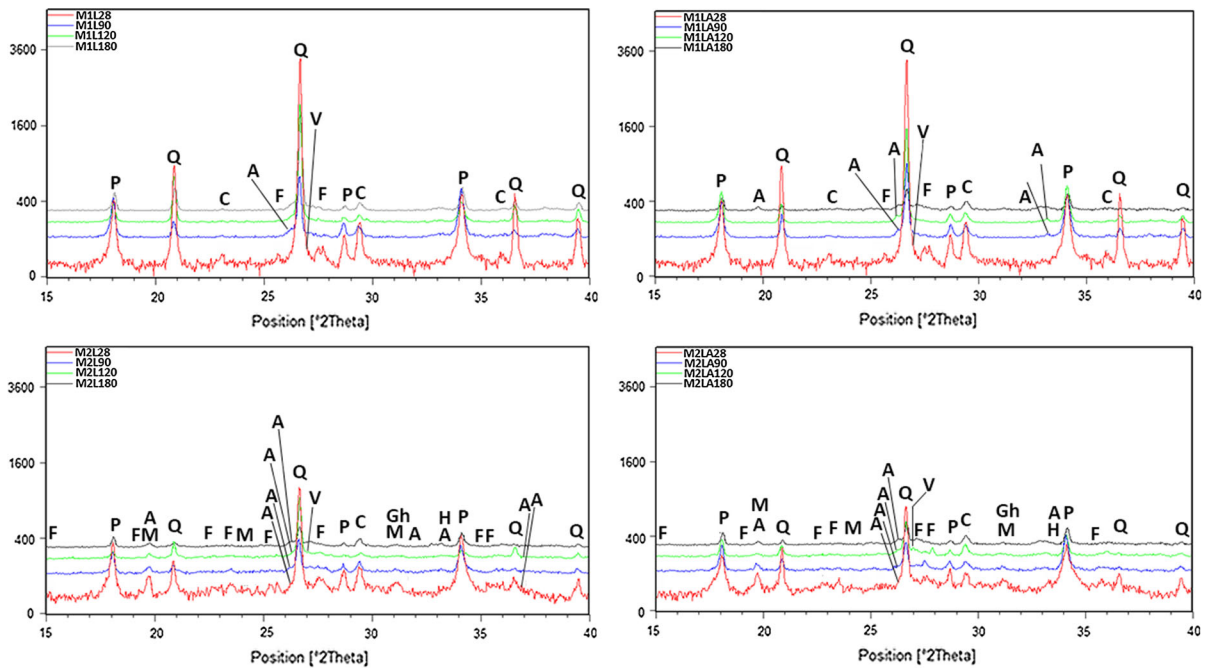


Fig. 2 Diffractograms of the specimens after 28, 90, 120 and 180 days of curing (Notation: Q: Quartz, P: Portlandite, C: Calcite, F: Feldspar, M: Mica, H: Hematite, Gh: Gehlenite, A: Aragonite, V: Vaterite)

between 380 and 450 °C to the dehydration of portlandite, and between 580 and 700 °C to the decomposition of carbonates (Table 1) [43, 63].

Carbonation may also start during the mortar preparation [63], therefore the ratios of calcite and portlandite of the initial lime putty are necessary for accurate calculation of the consumption of portlandite.

To evaluate the evolution in carbonation and hydration reactions with aging, the portlandite consumption in carbonation reaction and in an eventual pozzolanic reaction was determined using the weight losses (WL) obtained by TGA–DSC analysis. Equations (1)–(4) explain the steps considered where C is used for content, WL is used for corresponding weight loss (%), and MM is used for the molar mass. C_{free} is the free portlandite content that is not involved in any reaction. $C_{\text{carbonation}}$ is the content of portlandite consumed in carbonation reactions, and $C_{\text{initial lime}}$ is the initial portlandite content.

$$C_{\text{free}} = (\text{WL}_{\text{Ca(OH)}_2} \times \text{MM}_{\text{Ca(OH)}_2}) / \text{MM}_{\text{H}_2\text{O}} \quad (1)$$

$$C_{\text{carbonation}} = (\text{WL}_{\text{CO}_2} \times \text{MM}_{\text{CaCO}_3}) / \text{MM}_{\text{CO}_2} \quad (2)$$

$$C_{\text{carbonation formed}} = (C_{\text{carbonation}} - C_{\text{initial lime}}) \quad (3)$$

$$C_{\text{carbonation consumption}} = (C_{\text{carbonation formed}} / C_{\text{initial lime}}) \times 100 \quad (4)$$

The portlandite consumption was very low in the M2 mortars at early ages, and similar to all other mortars at 180 days. Regarding the accelerator effect (M1L vs. M1LA), its influence was more pronounced at early ages (28 days) than at later ages.

The weight losses below 200 °C can indicate the presence of pozzolanic compounds or hygroscopic water inside the ceramics, which was higher in the M2 mortar than in the M1 non-treated samples at 28 days, but decreased at other ages, whereas in the specimens with accelerator, the difference in hydraulic activity was not pronounced (Table 1).

In all types of mortars at the end of 180 days, a decrease in portlandite and an increase in calcite were obtained as expected. In M1 mortars higher carbonation appears to occur earlier in control samples and in M2 mortars they almost went on equal terms. The effects of DEC on the acceleration of carbonation were not pronounced, but carbonation rate was steadier.

Table 1 The results of TGA–DSC analysis (WL: weight loss)

Mortar identification	Age (days)	WL < 200 °C	WL 380–500 °C	WL 580–700 °C	Ca(OH) ₂ (%)	CaCO ₃ (%)
M1L	28	1.38	3.16	3.37	12.99	7.66
	90	2.07	2.39	6.26	9.83	14.23
	120	1.07	1.93	6.74	7.93	15.32
	180	0.55	1.26	7.23	5.18	16.43
M1LA	28	3.14	3.61	4.10	14.84	9.32
	90	1.84	3.14	5.39	12.91	12.25
	120	1.32	2.59	6.86	10.65	15.59
	180	1.58	1.2	6.98	4.93	15.86
M2L	28	2.6	3.05	3.54	12.54	8.05
	90	2.19	2.66	5.66	10.94	12.86
	120	2.16	1.32	6.81	5.43	15.48
	180	1.32	1.12	9.11	4.60	20.70
M2LA	28	2.67	3.15	3.62	12.95	8.23
	90	2.19	2.54	5.97	10.44	13.57
	120	1.86	1.75	8.29	7.19	18.84
	180	1.38	1.46	9.39	6.00	21.34

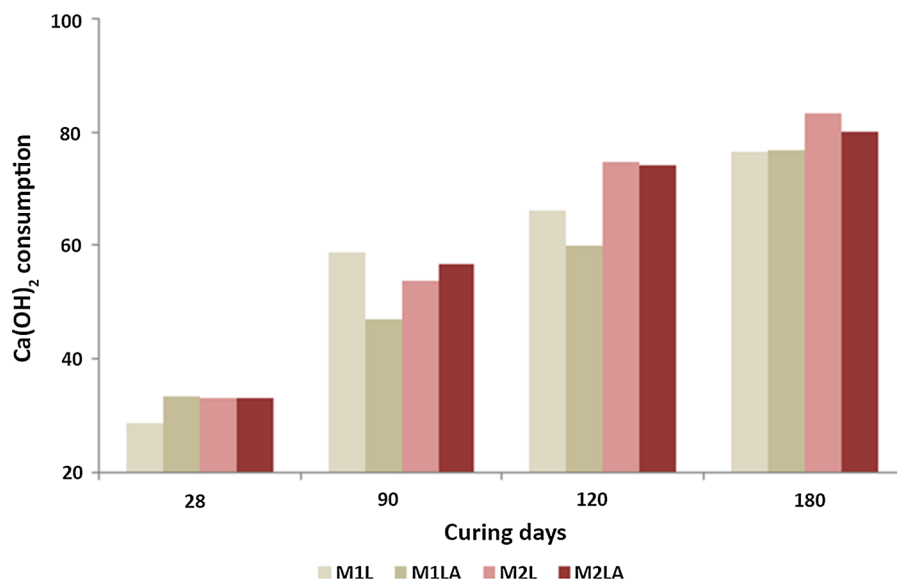
As can be seen from Table 1, the calcite formation was more pronounced in the M2 mixes, which coincides with the difference in portlandite consumption (Fig. 3).

3.2 Microstructural analysis

Observation of the mortar samples with the SEM found acicular aragonite crystals and nano-size

spherical vaterite crystals on the portlandite crystals, which corresponds to the traces of these minerals identified in the XRD patterns (Figs. 2, 4). In addition, the EDS spectra of the acicular crystal revealed a mainly calcium product (with small amounts of aluminum and silicon). Previous studies have found formations of different polymorphs of calcium carbonate, such as stable calcite in smaller sizes or less stable aragonite or vaterite in larger sizes [40]. The

Fig. 3 Portlandite consumption with curing age



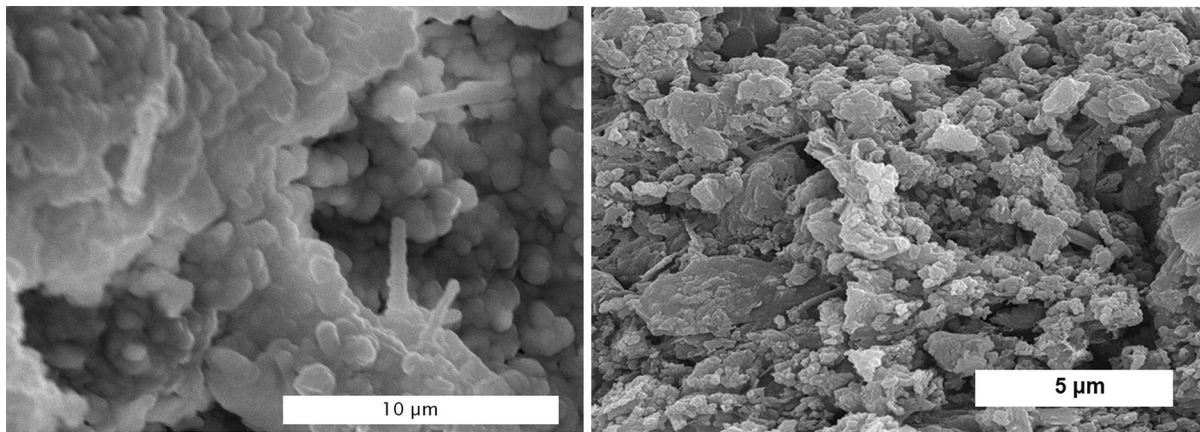


Fig. 4 SEM images of MILA90 (left) showing the rounded calcite crystals, acicular aragonite crystals, hexagonal portlandite crystals, and above all, vaterite crystals. M2LA180

(right) showing ruined morphology with the vaterite crystals on top of the modified scalenohedral calcite, acicular aragonite crystals and amorphous calcium carbonates

precipitation of CaCO_3 polymorphs and their size and morphology depend on several parameters such as temperature, water content, additives, pH and ion concentration [67]. Among the metastable CaCO_3 polymorphs, low temperature environments favor vaterite formation, while aragonite is preferably generated in high temperature environments [68]. In the SEM observations, both of them were detected in all samples.

The effect of accelerator on the microstructure was more visible in the M1 mortars with a rounded form in the crystal shape, which was very obvious at 90 days (Fig. 4). Later on, it turned into rounded edge modified scalenohedral crystals at 120 days, and amorphous calcium carbonate (ACC) appeared at 180 days next to the other calcium hydroxide and carbonate crystals. On the other hand, in the accelerator sprayed M2 mortars at early ages, aragonite, vaterite and portlandite were present. Later on, ACC formation next to needlelike aragonite was seen at 120 and 180 days, as it did in the control mortars.

The accelerator sprayed samples' crystals increased in size in the M1 mortars and on the contrary, grew smaller in the M2 mortars (Fig. 4). The research of Arizzi et al. [40] found that CaloSil leads to 1.8–2.8 μm aciform aragonite crystals and nano size tabular calcite crystals. The research of Gomez Villaba et al. [69, 70] detected 2.2 μm size aragonites and nano size rhombohedral calcite crystals. Without the precursor nanolime Calosil, a single use of

DiloCarB appears to lead to larger size crystals even in low relative humidity curing conditions.

The extent of these acicular crystals in MILA was 7.5 μm at 28 days and then fell to 4 μm at 90 days. On the other hand, the length of the needlelike crystals reached 10 μm in the MILA mortars at 90 days (Fig. 4). At 120 days, their length fell to 0.7 μm , and they were less abundant. Modified scalenohedral shape carbonate crystals proliferated on them in the MILA mortars at 180 days alongside 5 μm acicular crystals.

Flaky portlandite crystals were dominant in both of the L mortars, whereas at 120 days, at a 2.72 mm depth from the surface of the M2L sample, scalenohedral shape calcite crystals (1.7 μm in size) were observed. On the other hand, rounded edged hexagonal prism calcite crystals, together with platelike portlandite crystals, were observed in the M2LA sample (Fig. 4) [26, 71]. Among the control mortars at the end of the experiment, the MIL mortars' carbonation reached 3.08 mm from the surface while stick shaped crystals (5 μm) and calcite crystals with irregular morphology were observed at 4.10 mm from the surface in the M2L mortars (Fig. 5). The lower humidity during the curing of the samples caused not very well defined crystal morphologies [72].

3.3 Pore size distribution

Pore size distributions measured by MIP showed bimodal distribution in all four types of mortars

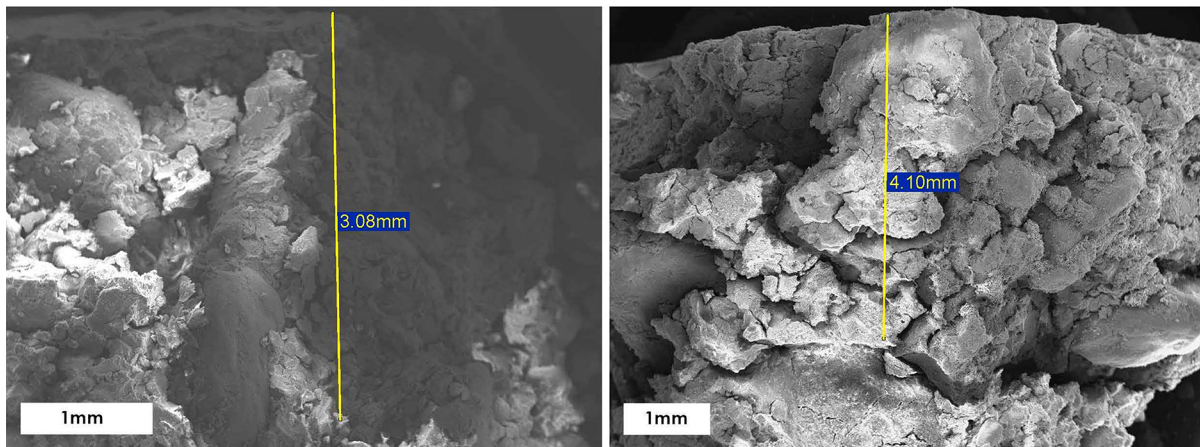


Fig. 5 SEM images of the control samples after 6 months (M1L on the left, M2L on the right, the yellow line indicates the distance of the detected calcite crystals from the surface)

(Fig. 6). They were mainly gathered in a higher percentage of pores less than $1\ \mu\text{m}$ in the M2 mortars, possibly due to the hydraulic compounds formed in the mortars with ceramic aggregates, which caused these mortars to have a smaller mean pore size and specific surface area than the M1 mortars. In addition, the porosity of the M2 mortar was greater than that of the M1 mortar at the beginning of the carbonation process, mainly because ceramic fragments are much more porous than sand, and the amount of entrained air was higher (Fig. 6, Table 2).

Pores between 0.1 and $100\ \mu\text{m}$ are capillary pores that contribute to water transfer through capillary action. Capillary pores are interconnected and cause moisture and air transfer [16, 17, 73, 74]. Small capillary pores ($< 1\ \mu\text{m}$) are formed in the binder when water evaporates, and larger capillary pores are formed in the spaces between binder and aggregate [16].

Sorption pores ($< 0.1\ \mu\text{m}$) are gel pores that develop in hydrated phases [16, 72] and coarser pores above $100\ \mu\text{m}$ that form as entrapped air in the mixing process, causing water intake due to permeability [73, 74].

Pores around $0.1\ \mu\text{m}$ in diameter are associated with the portlandite transformation to calcite [75]. With the transformation of portlandite to calcite and the consequent rise in volume, the largest and the smallest pores are plugged and total porosity falls [76]; although there is not noteworthy change in pore size distribution [16, 17, 73, 74], some modifications occur. The most noticeable change was seen in the

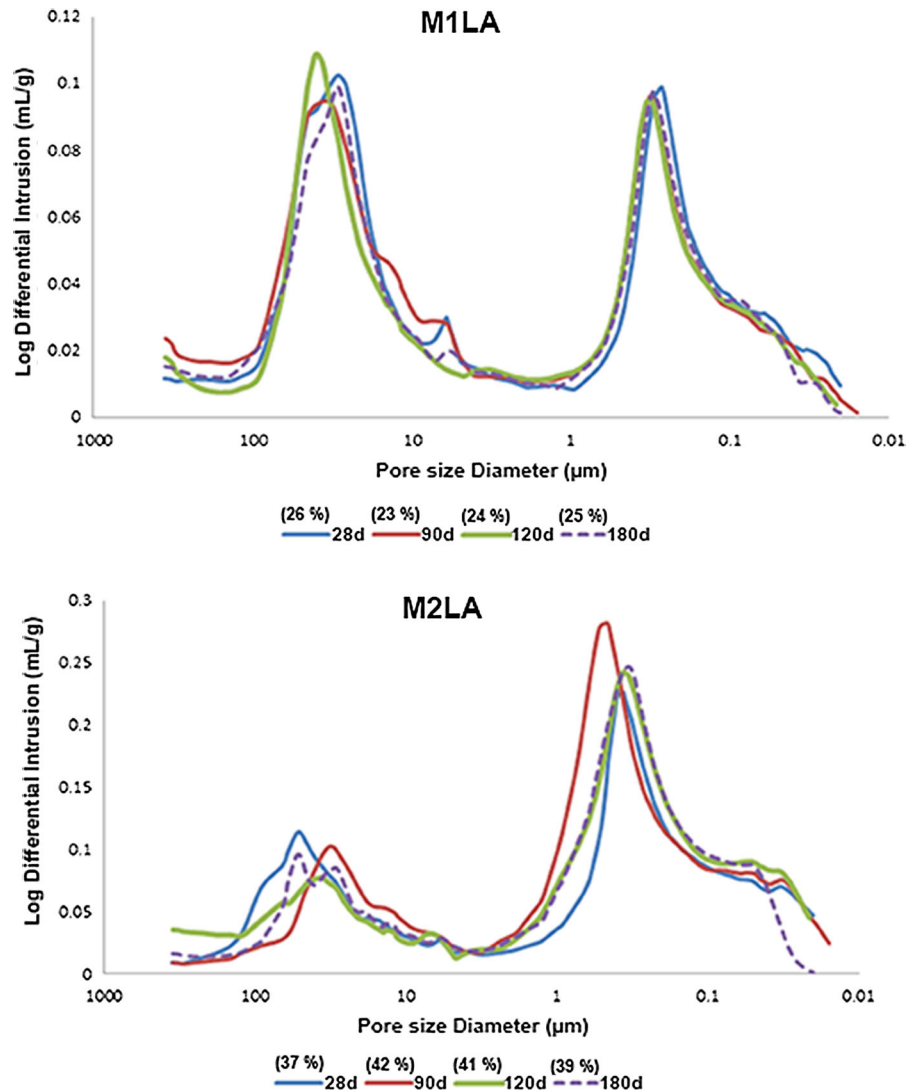
first modal of M1L mortars and in the second modal of M2LA mortars. Figure 6 shows how at 120 days the porosity between 20 and $8\ \mu\text{m}$ disappeared in the M1L and M1LA mortars, and the tendency of the M1L's larger pores to fall in size, from 70 to $30\text{--}40\ \mu\text{m}$ with no significant changes in pores of less than $1\ \mu\text{m}$ in size.

In the M2 mortars, the number of the macropores ($100\text{--}10\ \mu\text{m}$) was lower than that of the M1 mortars, and their size and amount fell with age. Large pores ($> 50\ \mu\text{m}$) occurred when the aggregate shapes were rounded, resulting in bad cohesion between the lime and the aggregate and causing a reduction in strength [10]. In the M2LA samples, the number of micropores ($< 1\ \mu\text{m}$) was higher than that of the M2L sample, which also slightly decreased. Sorption pores below $0.1\ \mu\text{m}$ decreased at 180 days (Fig. 6).

In the mortars with the accelerator additive, there were no significant variations of porosity with curing, whereas the M1L mortar's porosity increased at 180 days due to cracking caused by shrinkage of the binder that was observed under the optical microscope. In the case of the M2L mortar, porosity significantly decreased at 180 days due to the formation of new mineral phases (calcite, aragonite, vaterite) inside the pore system (Fig. 7).

Porosity can be augmented due to: (a) an increase in the amount of pores, or (b) increased pore size [73]. In our case, the former was seen in the M1L mortars, and the latter was observed in the M2LA mortars.

Fig. 6 Evolution of the pore size distributions of the mortars with aging (porosity values are shown in the legend with the corresponding age)



3.4 Physical and hydric properties

The ultrasonic pulse velocity (UPV) of the mortars without the DEC additive continually increased with advancing age to 180 days, reaching gains of 13.5% in the M1L and 6.2% in the M2L mortars. On the other hand, the mortars with carbonation accelerator did not undergo a significant change, fluctuating between slight decreases and slight increases. Moreover, these mortars had much lower UPV values at all ages than the mortars without carbonation accelerator. The mortars with ceramic aggregates had, in all cases in the first 120 days, slightly higher values for ultrasonic

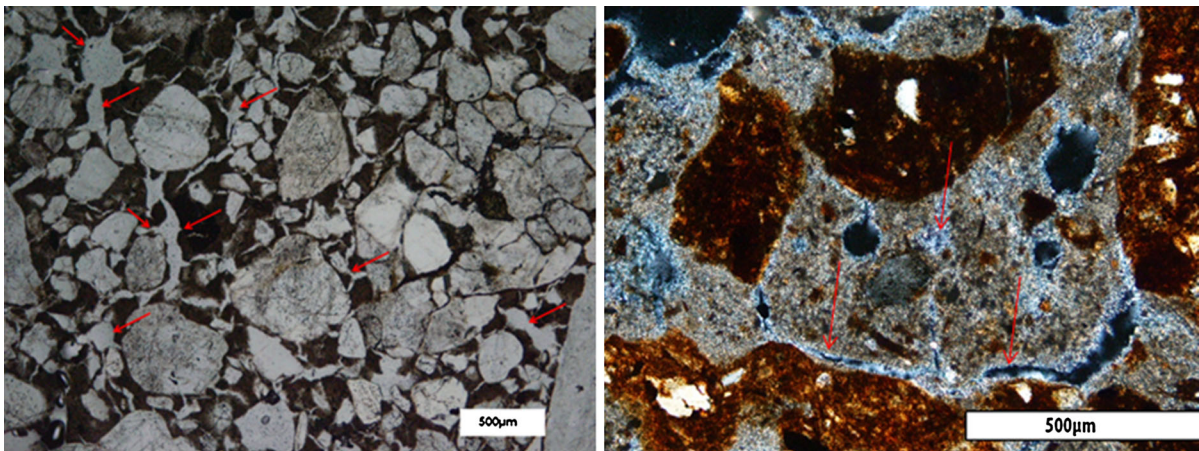
velocity, which can be attributed to their hydraulic characteristics.

Since carbonation begins in the exterior layer, as time passes the surface hardness is supposed to increase. In fact, the surface hardness increased in the first 120 days of carbonation in all the curing conditions (Table 2) with an increase of 4% in the M1 mortars and 5% in the M2 mortars. At 180 days, the only mortar that increased in hardness was the M2LA mortar with an increase of 9%. Following the same trend as ultrasonic velocity, the M2 mortars had higher surface hardness than the M1 mortars.

This confirms that the incorporation of brick-tile dust and fragments increased the hardness of the

Table 2 The physical properties of the mortar samples at 28, 90, 120 and 180 days of curing

Mortars identification	Ultrasonic velocity (m/s)				Surface hardness (LH)				Air permeability (mD)			
	28 d	90 d	120 d	180 d	28 d	90 d	120 d	180 d	28 d	90 d	120 d	180 d
M1L												
Average	1335	1479	1502	1516	206	211	214	205	1803	2404	3421	3052
SD	84	83	103	92	6	5	2	5	779	525	193	367
M1LA												
Average	1090	1060	1094	1070	211	214	219	217	1666	2335	2267	2804
SD	79	63	67	53	1	3	8	2	714	791	426	968
M2L												
Average	1421	1490	1558	1509	211	216	220	219	2234	2914	3509	2560
SD	89	84	93	66	4	2	7	34	786	1887	1230	725
M2LA												
Average	1113	1066	1121	1071	213	224	225	233	1400	2243	2366	3105
SD	117	60	73	72	12	4	1	6	308	777	755	1690

**Fig. 7** A thin section image of an M1L mortar specimen (left) and an M2L mortar specimen (right) at 180 days showing the crack pattern (cracks are indicated by arrows). This image was generated by polarized optical microscopy (POM) with parallel nicols

mortars [77] and appeared to be even better with the application of a carbonation accelerator.

Unlike surface hardness, the air permeability of all the mortars increased during the curing process. Only in the M2L mortars was the increase disrupted at 180 days with a sudden fall (Table 2). The increase in air permeability may be due to the increase in total porosity because the change in the amount of pore sizes between 0.1 and 1 μm has an influence on it [27]. As with porosity, the M2 mortars had generally higher air permeability than the M1 mortars.

The saturation degree and open porosity by vacuum tended to decrease during the carbonation process. In the M1 mortars, slight decreases were observed at the end, while the highest decreases occurred in the M2 mortars with sudden falls at 180 days of carbonation. Their water absorption capacity consistently fell. The decrease of open porosity was 27.2% without carbonation accelerator and 29.1% with accelerator, whereas in the M1 mortars, the reductions were 3.5 and 2.9%, respectively (Table 3).

The capillarity coefficients decreased only in the M2 mortar with carbonation accelerator, while the

Table 3 The hydric properties of the mortars at 28, 90, 120 and 180 days of curing

Mortars identification	Saturation (%)				Open porosity (%)				Capillarity coefficient (kg/m ² min ^{0.5})			
	28 d	90 d	120 d	180 d	28 d	90 d	120 d	180 d	28 d	90 d	120 d	180 d
M1L												
Average	17.4	17.2	17.2	16.4	31.1	31.0	31.1	29.9	9.0	10.2	9.3	10.0
SD	0.5	0.5	0.6	0.2	0.6	0.6	0.7	0.3	3.6	0.4	0.1	0.4
M1LA												
Average	17.0	16.8	16.8	16.2	30.6	30.5	30.8	29.6	9.6	10.5	10.5	10.2
SD	0.1	0.3	0.3	0.3	0.2	0.4	0.7	0.5	0.2	0.8	0.7	0.8
M2L												
Average	35.4	34.7	33.8	22.7	48.1	47.7	47.1	34.7	17.6	20.7	18.0	19.2
SD	0.1	0.1	0.1	1.0	0.1	0.1	0.1	1.3	1.1	3.0	0.8	0.7
M2LA												
Average	36.3	35.6	34.6	22.6	48.7	48.5	47.8	34.4	21.9	21.0	18.4	18.9
St. dev	1.0	1.1	1.1	2.0	0.6	0.8	0.8	2.3	2.2	1.6	1.1	0.3

coefficients of the rest of the samples showed fluctuations or no significant change with advancing age (Table 3). This hydric behavior of the mortars is related to the modification of their pore system, where there is a filling of some pores by the formation of calcium carbonate phases after the lime penetrates into the ceramic aggregates [78]. The abundance of the unstable calcium carbonate polymorphs and fluctuations in the laboratory conditions may have affected the fluctuations in the capillary coefficients as well.

3.5 Mechanical properties

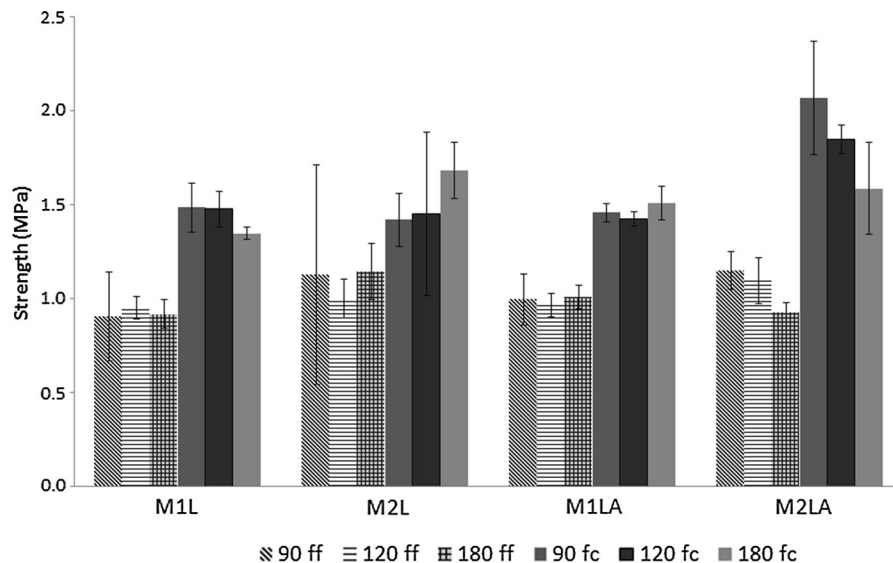
As Fig. 8 shows, the uniaxial compressive strength values were around 1.5 MPa, and no considerable change was observed until 180 days. The M2LA mortars differed from the others with remarkably higher values and a greater fall in strength at 180 days as well. The M1 mortars had the lowest flexural strength values, below 1 MPa, the M2 mortars had higher values (Fig. 8) following the same trend as ultrasonic velocity and superficial hardness (Table 2). While there was no significant change in the flexural strength of the M1 mortars, the effect of carbonation accelerator was observed in the samples with ceramics added. The falling flexural strength seen in the M2LA samples may have been caused by cracking due to shrinkage [10, 79, 80].

Veiga et al. [81] have reported that the range of compressive strength for repair mortars for old masonry should be between 0.4 and 2.5 MPa, and that flexural strength should be between 0.2 and 0.7 MPa. In a study by Matias et al. [82], the values obtained for lime mortars without and with ceramic waste aggregates were between 0.2 and 1.5 MPa for compressive strength and between 0.2 and 0.3 MPa for flexural strength, and always higher for mortars with ceramic aggregate. Çizer et al. [83] found that flexural strength was similar in dry curing environments (0.4–0.8 MPa) and higher in humid environments (0.75–2.15 MPa).

Increased total porosity results in a fall in the compressive strength [73]. The fall in the compressive strength values of the M1L and M2LA mortars in time may have been related to this phenomenon. Mechanical strength is mainly influenced by the coarser pores and by cracks [84]. Concerning the range of the pores that can be detected by MIP, in the M2LA mortar it can be seen that the peak of the large capillary pores (10–100 µm) was higher and have larger volume at 180 days compared with 90 and with 120 days. In the case of M1L the fall in mechanical strength can be explained by cracking due to shrinkage of the binder which was observed under optical microscope.

As long as stable compounds form, porosity falls and the strength of mortars increases [74]. The amorphous silica and aluminosilicates in Roman

Fig. 8 The flexural strength (ff) and compressive strength (fc) of the samples with aging



bricks can promote the chemical reaction with the hydrated lime and also physically contribute to their bonding [85–87], explaining the better mechanical characteristics of the M2 mortars. The C–S–H formations contribute more than the CaCO_3 phases in the mechanical strength development of these mortars [83]. Immediately after the hydration reaction, when the carbonation reaction occurs both in the lime and the hydrated phases, cause their decalcification in the form of more calcium carbonate (calcite, vaterite and aragonite) crystals. Highly pozzolanic reactions did not occur either because of the dry curing conditions or the low pozzolanic level of the Roman ceramics, so the greater fall in the strength of the M2LA mortars could be ascribed to shrinkage due to the re-precipitation of new calcium carbonate crystals.

4 Conclusion

Overall, using ceramic aggregate in lime mortars is advantageous because it contributes to better aggregates bonding and mortars higher mechanical properties. The use of fine ceramic particles and dust also enhances the hydration and carbonation reactions due to their larger specific surface area and higher porosity. The samples with sand and ceramic aggregate (M2) had formed more stable phases of calcium carbonate polymorphs, with aragonite in the earlier stages of curing, as was observed using XRD and

SEM. Apparently, the curing conditions favored the early formation of aragonite in the presence of the clay minerals and lime. Here, the morphology of the silicate minerals also had an important role. Since the sand has a tight crystalline form, the lime binder cannot cling and react, whereas the ceramic, especially Roman ceramic, has amorphous silica, which allows the alkaline binder to enter and react [87]. Nevertheless, and contrary to expectations, the Roman ceramics from Complutum contain high temperature minerals (e.g., mullite and gehlenite), the amorphousness of which is not enough to promote pozzolanic reactions.

The use of the diethyl carbonate additive on the mortars aids the carbonation process, promoting a higher amount of calcite and aragonite formation. It is also important to note that, in the mortars with only siliceous sand as aggregate, the DEC caused rounded crystal morphology, whereas in the mortars with ceramic aggregate, less defined morphology was present. This is probably why the ultrasonic pulse velocity values in the mortars with ceramic aggregate only exhibited fluctuations, and the difference between the accelerator sprayed mortars was so small. However, in the mortars without ceramic aggregate, the augmentation in the velocity with advancing age was more obvious. The other clear effect of DEC is that it enhances surface hardness, especially when the mortar has ceramics components as the M2 mortars did. The increase in surface hardness until 180 days and then its sudden reduction showed that cracks

occurred in the interior of the mortar specimen until 6 months, and that at 6 months superficial cracks occurred as well. This hypothesis does not include the M2LA mortars because their surface hardness consistently increased and never fell. Apparently, the microcracks observed in the other analyses did not reach their surface. In addition, a higher reduction in open porosity accessible to water is occurred in the mortars with ceramic aggregates. This could be due to the formation of hydrated products, which reduce porosity, thus improving mechanical strength and superficial hardness as well as resistance to water-related deterioration. The use of carbonation accelerator caused higher compressive strength in the mortars with sand and ceramic. The fall in mechanical strength at 120 days in all the samples may be related to the shrinkage cracks and microcracks that occur due to rapid drying in accelerated carbonation and the volume increase of the portlandite-calcium carbonate transformation as a result of its carbonation and/or poor water/binder ratio due to the evaporation caused by the heat generated during the carbonation reaction. The reason the M1 mortars had lower strength values is probably related to poor microstructure, which did not involve hydrated phases. Although all the samples' porosity decreased for 4 months, the most remarkable reduction in porosity was observed in those with the carbonation accelerator.

The fluctuations in the portlandite and calcite amounts determined using TGA–DSC can be associated with some overlapping of the dehydration of portlandite and the decomposition of unstable CaCO_3 polymorphs, and those in XRD can be explained by the different carbonation degrees in different specimens or inhomogeneity in the same specimens.

The lime mortars on which the carbonation agent DiloCarB was sprayed exhibited better physical and hydric properties when they included ceramic particles and dust. The mechanical strength results also indicated that the samples with ceramic aggregate and accelerator had higher resilience than the control samples.

Acknowledgements The authors would like to acknowledge D. Francisco González Yunta from PROIESCON for the supply of lime putty. They would also like to thank Tom Kelso for language revision and the anonymous reviewers for their valuable comments and suggestions to improve the quality of the article. The mortar samples were manufactured at Construction Laboratory UPM ETSAM, and the analyses were

conducted at the Petrophysics Laboratory of the Instituto de Geociencias (CSIC-UCM).

Funding This study was funded by project CLIMORTEC (BIA2014-53911-R) of Ministry of Economy and Competitiveness of Spain and the program Geomateriales2 (S2013/MIT2914) of the Community of Madrid.

Compliance with ethical standards

Conflict of interest The authors declare that they have no conflict of interest.

References

1. Paiva H, Velosa A, Veiga R (2010) Effect of maturation time on the fresh and hardened properties of an air lime mortar. *Cem Concr Res* 40:447–451
2. Moorehead DR (1986) Cementation by the carbonation of hydrated lime. *Cem Concr Res* 16(5):700–708
3. Dheilly RM, Tudo J, Sebaibi Y, Quéneudec M (2002) Influence of storage conditions on the carbonation of powdered $\text{Ca}(\text{OH})_2$. *Constr Build Mater* 16:155–161
4. Martínez Ramírez S, Sánchez Cortes S, García Ramos JV, Domingo C, Fortes C, Blanco Varela MT (2003) Micro-Raman spectroscopy applied to depth profiles of carbonates formed in lime mortar. *Cem Concr Res* 33:2063–2068
5. Ferreti D, Bazant ZP (2006) Stability of ancient masonry towers: moisture diffusion, carbonation and size effect. *Cem Concr Res* 36:1379–1388
6. Franzini M, Leoni L, Lezzerini M (2000) A procedure for determining the chemical composition of binder and aggregate in ancient mortars: its application to mortars from some medieval buildings in Pisa. *J Cult Herit* 1:365–373
7. Peroni S, Tersigni C, Torraca G, Cerea S, Forti M, Guidobaldi F, Rossi-Doria P, De Rege A, Picchi D, Pietrafitta FJ, Benedetti G (1982) Lime based mortars for the repair of ancient masonry and possible substitutes. In: *Mortars, cements and grouts used in the conservation of historic buildings*, Rome, pp 63–99
8. Luxan M, Dorrego F, Laborde A (1995) Ancient gypsum mortars from St. Engracia (Zaragoza, Spain) characterization-identification of additives and treatments. *Cem Concr Res* 25(8):1755–1765
9. Callebaut K, Elsen J, Van Balen K, Viaene W (2001) Nineteenth century hydraulic restoration mortars in the Saint Michael's Church (Leuven, Belgium). Natural hydraulic lime or cement. *Cem Concr Res* 31:397–403
10. Lanás J, Álvarez-Galindo JI (2003) Masonry repair lime-based mortars: factors affecting mechanical behaviour. *Cem Concr Res* 33(11):1867–1876
11. Varas MJ, Álvarez de Buergo M, Fort R (2007) The origin and development of natural cements: The Spanish experience. *Constr Build Mater* 21(2):436–445
12. O'Brien PF, Bell E, Pavia Santamaria S, Boyland P, Cooper TP (1995) Role of mortars in the decay of granite. *Sci Total Environ* 167:103–110



13. Moropoulou A, Bakolas A, Anagnostopoulou S (2005) Composite materials in ancient structures. *Cem Concr Compos* 27:295–300
14. Perez Ema N, Alvarez de Buergo M, Bustamante R (2013) Effects of conservation interventions on the archaeological Roman site of Merida (Spain). *Adv Res Procedia Chem* 8:269–278
15. Varas-Muriel MJ, Pérez-Monserrat EM, Vázquez-Calvo C, Fort R (2015) Effect of conservation treatments on heritage stone. Characterization of decay processes in a case study. *Constr Build Mater* 95:611–622
16. Lourenço PB, van Hees R, Fernandes F, Lubelli B (2014) Characterization and damage of brick masonry. In: Costa A, Guedes J, Varum H (eds) *Structural rehabilitation of old buildings. Building Pathology and Rehabilitation*, vol 2. Springer, Berlin, Heidelberg
17. Groot C (2016) Repair mortars for historic masonry: effects of the binder choice on durability. *HERON* 61(1):33–56
18. Ventolà L, Vendrell M, Giraldez P, Merino L (2011) Traditional organic additives improve lime mortars: new old materials for restoration and building natural stone fabrics. *Constr Build Mater* 25:3313–3318
19. Fang S, Zhang K, Zhang H, Zhang B (2015) A study of traditional blood lime mortar for restoration of ancient buildings. *Cem Concr Res* 76:232–241
20. Rampazzi L, Colombini MP, Conti C, Corti C, Lluveras-Tenorio A, Sansonetti Z (2016) Technology of medieval mortars: an investigation into the use of organic additives. *Archaeometry* 58(1):115–130
21. Martínez-Ramírez S, Puertas F, Blanco-Varela MT (1995) Carbonation process and properties of a new lime mortar with added sepiolite. *Cem Concr Res* 25:39–50
22. Aggelakopoulou E, Bakolas A, Moropoulou A (2011) Properties of lime-metakaolin mortars for the restoration of historic masonries. *Appl Clay Sci* 53:15–19
23. Vejmelková E, Keppert M, Rovnaníková P, Keršner Z, Černý R (2012) Application of burnt clay shale as pozzolan addition to lime mortar. *Cem Concr Compos* 34:4486–4492
24. Andrejkovičová S, Velosa A, Gameiro A, Ferraz E, Rocha F (2013) Palygorskite as an admixture to air lime-metakaolin mortars for restoration purposes. *Appl Clay Sci* 83–84:368–374
25. Blanco-Varela MT, Fortes-Revilla C (2004) Effect of chemical admixtures on lime-metakaolin mortars characteristics. *Coalition* 7:8–11
26. Cultrone G, Sebastián E, Ortega Huertas M (2005) Forced and natural carbonation of lime-based mortars with and without additives: mineralogical and textural changes. *Cem Concr Res* 35:2278–2289
27. Arizzi A, Cultrone G (2012) Aerial lime-based mortars blended with a pozzolanic additive and different admixtures: a mineralogical, textural and physical-mechanical study. *Constr Build Mat* 31:135–143
28. Izaguirre A, Lanás J, Álvarez JI (2011) Characterization of aerial lime-based mortars modified by the addition of two different water-retaining agents. *Cem Concr Compos* 33:309–318
29. Izaguirre A, Lanás J, Álvarez JI (2009) Effect of water-repellent admixtures on the behavior of aerial lime-based mortars. *Cem Concr Res* 39:1095–1104
30. Fernández JM, Duran A, Navarro-Blasco I, Lanás J (2013) Influence of nanosilica and a polycarboxylate ether superplasticizer on the performance of lime mortars. *Cem Concr Res* 43:12–24
31. Pérez-Nicolás M, Duran A, Navarro-Blasco I, Fernández JM, Sirera R, Alvarez JI (2016) Study on the effectiveness of PNS and LS superplasticizers in air lime based mortars. *Cem Concr Res* 82:11–22
32. Jasiczak J, Zielinski K (2006) Effect of protein additive on properties of mortar. *Cem Concr Compos* 28:451–457
33. Sickels LB (1981) Organics versus synthetics: their use as additives in mortars. In: *Mortars, cements and grouts used in the conservation of historic buildings. Symposium ICCROM, Rome*, pp 25–52
34. Álvarez JI, Fernández JM, Navarro-Blasco I, Duran A, Sirera A (2013) Microstructural consequences of nanosilica addition on aerial lime binding materials: influence of different drying conditions. *Mater Charact* 80:36–49
35. Theodoridou M, Charalambous E, Maravelaki-Kalaitzaki P, Ioannou I (2016) Amelioration of crushed brick - lime composites using nano-additives. *Cem Concr Compos* 68:77–87
36. Stefanidou M, Tsardaka E-C, Pavlidou E (2017) Influence of nano-silica and nano-alumina in lime-pozzolan and lime-metakaolin binders. *Mater Today Proc* 4:6908–6922
37. Campbell AS (2013) Consolidant particle transport in limestone, concrete and bone, PhD dissertation, Institute for Materials and Processes School of Engineering University of Edinburgh
38. Daehne A, Herm C (2013) Calcium hydroxide nanosols for the consolidation of porous building materials -results from EU-STONECORE. *Herit Sci* 1:11
39. Slížková Z, Drdáký M (2014) Testing of treatment effects of nano sols on selected porous historic materials. In: *International conference on conservation of stone and earthen architectural heritage*, p 289
40. Arizzi A, Gomez-Villalba L, Lopez-Arce P, Cultrone G, Fort R (2015) Lime mortar consolidation with nanostructured calcium hydroxide dispersions: the efficacy of different consolidating products for heritage conservation. *Eur J Mineral* 27(3):311–323
41. Faria P, Martins A (2013) Influence of air lime type and curing conditions on lime and lime-metakaolin mortars. In: *de Freitas V, Delgado J (eds) Durability of building materials and components. Building pathology and rehabilitation*, vol 3. Springer, Berlin, Heidelberg
42. Rodriguez-Navarro C, Cazalla O, Elert K, Sebastian E (2002) Liesegang pattern development in carbonating traditional lime mortars. *Proc R Soc Lond A* 458:2261–2273
43. Lanás J, Alvarez JI (2006) Study of the mechanical behavior of masonry repair lime-based mortars cured and exposed under different conditions. *Cem Concr Res* 36(5):961–970
44. Gameiro A, Santos Silva A, Faria P, Grilo J, Branco T, Veiga R (2014) Physical and chemical assessment of lime-metakaolin mortars: influence of binder:aggregate ratio. *Cem Concr Compos* 45:264–271
45. Grilo J, Faria P, Veiga R, Santos Silva A, Silva V, Velosa A (2014) New natural hydraulic lime mortars-Physical and microstructural properties in different curing conditions. *Constr Build Mat* 54:378–384



46. Çizer Ö, Van Balen K, Elsen J, Van Gemert D (2008) Carbonation reaction kinetics of lime binders measured using XRD. In: 2nd International conference on accelerated carbonation for environmental and materials engineering, 1–3 October 2008, Rome, Italy. Proceedings ACEME08, pp 139–148
47. Sánchez Moral S, García-Guinea J, Luque Luque L, González-Martín R, López-Arce P (2004) Carbonation kinetics in Roman-like lime mortars. *Materiales de Construcción* 54:275
48. Xiang L, Xiang Y, Wang ZG, Jin Y (2002) Influence of chemical additives on the formation of super-fine calcium carbonate. *Powder Technol* 126:129–133
49. Xiang L, Xiang Y, Wen Y, Wei F (2004) Formation of CaCO₃ nanoparticles in the presence of terpineol. *Mater Lett* 58:959–965
50. Ergenç D (2017) Roman mortars used in the archaeological sites in Spain and Turkey: a comparative study and the design of repair mortars. Unpublished Ph.D Dissertation, Universidad Politécnica de Madrid
51. CEN, EN 1015-2 (1998) Bulk sampling of mortars and preparation of test mortars, Brussels
52. UNE-EN 1936 (2007) Natural stone test methods-Determination of real density and apparent density, and of total and open porosity
53. Hall C, Hoff WD (2002) Water transport in brick, stone and concrete. Spon Press, London, p 318
54. UNE-EN 1015-18 (2003) Methods of test for mortar for masonry-Part 18: determination of water absorption coefficient due to capillary action of hardened mortar
55. UNE-EN 1015-11 (2007) Methods of test for mortar for masonry-Part 11: determination of flexural and compressive strength of hardened mortar
56. Hisashi A, Matsukura Y (2008) Estimating the unconfined compressive strength of intact rocks from Equotip hardness. *Bull Eng Geol Env* 67(1):23–29
57. Viles H, Goudie A, Grab S (2011) The use of the Schmidt Hammer and Equotip for rock hardness assessment in geomorphology and heritage science: a comparative analysis. *Earth Surf Proc Land* 36:320–333
58. Cleland DJ, Basheer PAM (1999) Adhesion and integrity of joints between construction materials. In: Puterman Y (ed) Second international RILEM symposium on adhesion between polymers and concrete, RILEM Publications SARL, pp 257–265
59. UNE 83-308-86 (1986) Ensayos de hormigón-Determinación de la velocidad de los impulsos ultrasonidos, Spain
60. Lanás J, Sirera R, Alvarez JI (2003) Compositional changes in lime-based mortars exposed to different environments. *Thermochim Acta* 429:219–226
61. Montoya C, Lanás J, Arandigoyen M, Navarro I, Casado PJ, Alvarez JI (2003) Study of Ancient dolomitic mortars of the church of Santa María de Zamarce in Navarra (Spain). Comparison with simulated standards. *Thermochimica Acta* 398:107–122
62. Lawrence RMH, Mays TJ, Walker P, D'Ayala D (2006) Determination of carbonation profiles in non-hydraulic lime mortars using thermogravimetric analysis. *Thermochim Acta* 444:179–189
63. Santos Silva A, Gameiro A, Grilo J, Veiga R, Velosa A (2014) Long-term behavior of lime-metakaolin pastes at ambient temperature and humid curing condition. *Appl Clay Sci* 88–89:49–55
64. Moropoulou A, Bakolas A, Bisbikou K (1995) Characterization of ancient, byzantine and later historic mortars by thermal and X-ray diffraction techniques. *Thermochim Acta* 269(270):779–795
65. Bonazza A, Ciantelli C, Sardella A, Pecchioni E, Favoni O, Natali I, Sabbioni C (2013) Characterization of hydraulic mortars from archaeological complexes in Petra. *Periodico di Mineralogia* 82(2):459–475
66. Genestar C, Pons C, Más A (2006) Analytical characterization of ancient mortars from the archaeological Roman city of Pollentia (Balearic Islands, Spain). *Anal Chim Acta* 557:373–379
67. Çizer Ö, Van Balen K, Elsen J, Van Gemert D (2008) Crystal morphology of precipitated calcite crystals from accelerated carbonation of lime binders. In: ACEME08, 2nd International conference on accelerated carbonation for environmental and materials engineering, Rome, pp 149–158
68. López-Arce P, Gómez-Villalba LS, Martínez-Ramírez S, Álvarez de Buergo M, Domingo C, Fort R (2011) Influence of relative humidity on the carbonation of calcium hydroxide nanoparticles and the formation of calcium carbonate polymorphs. *Powder Technol* 205(1–3):263–269
69. Gómez-Villalba LS, López-Arce P, Alvarez de Buergo M, Fort R (2011) Structural stability of a colloidal solution of a Ca(OH)₂ nanocrystals exposed to high relative humidity conditions. *Appl Phys A* 104(4):1249–1254
70. Gómez-Villalba LS, López-Arce P, Fort R (2012) Nucleation of CaCO₃ polymorphs from a colloidal alcoholic solution of Ca(OH)₂ nanocrystals exposed to low humidity conditions. *Appl Phys A* 106:213–217
71. Çizer Ö, Rodríguez-Navarro C, Ruiz-Agudo E, Elsen J, Van Gemert D, Van Balen K (2012) Phase and morphology evolution of calcium carbonate precipitated by carbonation of hydrated lime. *J Mater Sci* 47:6151–6165
72. Nobrega de Azeredo A, Struble LJ, Carneiro A (2015) Microstructural characteristics of lime-pozzolan pastes made from kaolin production wastes. *Mater Struct* 48:2123–2132
73. Thomson ML, Lindqvist, JE, Elsen J (2004) Porosity of historic mortars. In: 13th international brick and block masonry conference, Amsterdam
74. Papayianni I, Stefanidou M (2001) The evolution of porosity in lime based mortars. In: 8th euroseminar on microscopy applied to building materials, Athens
75. Lawrence RMH (2006) A study of carbonation in nonhydraulic lime mortars, University of Bath, Unpublished Ph.D. Dissertation
76. Izaguirre A, Lanás J, Alvarez JI (2010) Ageing of lime mortars with admixtures: durability and strength assessment. *Cem Concr Res* 40:1081–1095
77. Nežerka V, Slížková Z, Plachý T, Frankeová D, Petráňová V (2014) Comprehensive study on mechanical properties of lime-based pastes with additions of metakaolin and brick dust. *Cem Concr Res* 64:17–29
78. Nežerka V, Nemeček J, Slížková Z (2015) Investigation of crushed brick-matrix interface in lime-based ancient mortar by microscopy and nanoindentation. *Cem Concr Compos* 55:122–128

79. Farinha C, de Brito J, Veiga R (2015) Incorporation of fine sanitary ware aggregates in coating mortars. *Constr Build Mater* 83:194–206
80. Lanás J, Pérez Bernal JL, Bello MA, Álvarez Galindo JJ (2004) Mechanical properties of natural hydraulic lime-based mortars. *Cem Concr Res* 34:2191–2201
81. Veiga MR, Fragata A, Velosa AL, Magalhães AC, Margalha MG (2010) Lime-based mortars: viability for use as substitution renders in historical buildings. *Int J Archit Herit* 4(2):177–195. Philadelphia: Taylor and Francis. Paulo B. Lourenço and Pere Roca eds. Special Issue. ISSN 1558-3058. <https://doi.org/10.1080/15583050902914678>
82. Matias G, Faria P, Torres I (2014) Lime mortars with ceramic wastes: characterization of components and their influence on the mechanical behaviour. *Constr Build Mater* 73:523–534
83. Çizer Ö, Van Balen K, Elsen J, Van Gemert, D (2010) Competition between hydration and carbonation in hydraulic lime and lime-pozzolana mortars. *Adv Mater Res* 133–134, 241–246. Trans Tech Publications, Switzerland. <https://doi.org/10.4028/www.scientific.net/amr>
84. Papayianni I, Stefanidou M (2006) Strength-porosity relationships in lime-pozzolan mortars. *Constr Build Mater* 20(9):700–705
85. Franquelo M, Robador M, Ramírez-Valle V, Durán A, Jiménez de Haro M, Pérez-Rodríguez J (2008) Roman ceramics of hydraulic mortars used to build the Mithraeum house of Mérida (Spain). *J Therm Anal Calorim* 1(92):331–335
86. Stefanidou M (2016) Use of natural pozzolans with lime for producing repair mortars. *Environ Earth Sci* 75(9):758. <https://doi.org/10.1007/s12665-016-5444-5>
87. Stefanidou M, Papayiani I, Pachtá V (2015) Analysis and characterization of Roman and Byzantine fired bricks from Greece. *Mater Struct* 48(7):2251–2260